Supplementary Information (SI) for Environmental Science: Processes & Impacts.
This journal is © The Royal Society of Chemistry 2025

SUPPLEMENTARY INFORMATION

Electron Exchange Capacity of Dissolved Natural Organic Matter: Further Method Development and Interpretation using Square Wave Voltammetry in Dimethyl Sulfoxide

Jeffrey M. Hudson[1], Han Cao[2], Wenqing Xu[2], Paul G. Tratnyek[1]*

[1] OHSU/PSU School of Public Health, Oregon Health & Science University, 3181 SW Sam Jackson Park Road, Portland, OR 97239, United States

[2] Department of Civil and Environmental Engineering, Villanova University, Villanova, Pennsylvania 19085, United States

*Corresponding author:
Email: tratnyek@ohsu.edu, Phone: 503-346-3431

Environmental Science: Processes & Impacts

Supplementary Information file includes 33 pages, 13 Figures, 6 Tables, 6 Texts, and 7 References

1/13/25 10:26 AM

Contents

Text S1. Theoretical electron exchange capacity calculations of some model quinones. 3
Table S1. Descriptor table of calibrant shuttles and used in this study. 5
Figure S1. Stability window for 0.1M TBAPF in DMSO obtained via cyclic voltammetry..... 6
Figure S2. (**A**) Example of peak due to oxide reduction on a Pt working electrode during cyclic voltammetry, located at −0.7 V in the presence of a pyDOM sample, W300.. 7
Table S2. Comparison of peak areas obtained for shuttles and NOM with a Pt and GC working electrode.. 8
Scheme S1. Effect of solvent on quinone reduction, adapted from Quan et al.[2]..... 9
Figure S3. Influence of water cosolvent on redox properties of AQDS.. 10
Text S2. Experimental determination of calibrant and NOM electro adsorption..... 11
Figure S4. Coulometric plot showing sorption of NQS (black solid line, Qtot) to electrode (Qdl, grey line) during anodic sweep..... 11
Table S3. Monolayer sorption parameters for calibrant (NQS) and NOM sample shown in Figure 2. 13
Text S3. Quantification and previous calibration details of SWV method. 14
Table S4. *EDC* and *EAC* values obtained using MCA method, previous SWV calibration method, and values obtained in this study. 16
Figure S5. AQDS and ferrocene calibrations, with insets showing the resulting calibration curve (as PA versus n e^-). 17
Figure S6. Calibration curves of various model quinones and other redox standards. 18
Figure S7. (**A**) Original method used in Cao et al.[1] to obtain EEC values. 19
Text S4. Revised calibration protocol details of SWV method..... 20
Figure S8. (**A**) Rank of calibration slopes obtained via the original method used in Cao et al.[1].(**B**) Rank of calibration slopes obtained in the current method. 22
Table S5. Electrochemical parameters obtained for calibrant model compounds and some NOM samples used in this study. 23
Figure S9. All compiled efficiency (η) data versus the calibrant model compound used in the measurement sorted by the corresponding values of η.. 24
Text S5. Linking hydrodynamic properties of calibrants to response factors within our cell..... 25
Figure S10. Efficiency (η) values plotted versus their working electrode surface area (cm^2) to volume (mL) ratios.. 26
Figure S11. Efficiency (η) of individual calibrant model compounds in this study and literature sorted based on their electrochemical cell configurations..... 27
Text S6. Determining diffusion coefficients and electron transfer kinetics of calibrants and NOM in our cell. 28
Figure S12. Analysis of calibrant model compound and NOM diffusion coefficients..... 30
Figure S13. (**A**) NOM and pyDOM EEC values plotted versus O/C ratios. (**B**) NOM and pyDOM EECs plotted versus E2:E3 values. (**C**) NOM and pyDOM EECs plotted versus SUVA values. 31
Table S6. NOM bulk molecular properties obtained from spectroscopy in Cao et al.[1] 32
References..... 33

Text S1. Theoretical electron exchange capacity calculations of some model quinones.

Assuming there is 1 mole of the following material, the maximum electron exchange (defined as EDC_{max} or EAC_{max} in the main text) of a model compound can be calculated as the following:

1. Hydroquinone, $C_6H_6O_2$ (# of C: 6) EEC: 2 mol_{e-} / (6 × 12 g_c) = 0.028 mol_{e-}/g_c = 28 mmol e^- g_c^{-1}	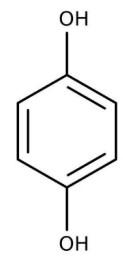
2. Juglone, $C_{10}H_6O_3$ (# of C: 10) EEC: 2 mol_{e-} / (10 × 12 g_c) = 0.0167 mol_{e-}/g_c = 16.7 mmol e^- g_c^{-1}	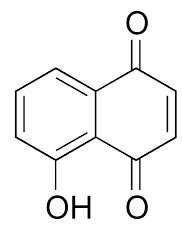

Based on comparisons between hydroquinone (1) to Juglone (2) the higher number of rings (more carbon) in the phenol indicates less EDC if they transfer the same electron.

However, if there are more than 2 mol_{e-} per mole:

3. Quercetin, $C_{15}H_{10}O_7$ (polyphenol, # of C: 15) (*assuming each -OH/=O is redox active*) EEC: 6 mol_{e-} / (15 × 12 g_c) = 0.0333 $mmol_{e-}/g_c$ = 33.3 mmol e^- g_c^{-1}	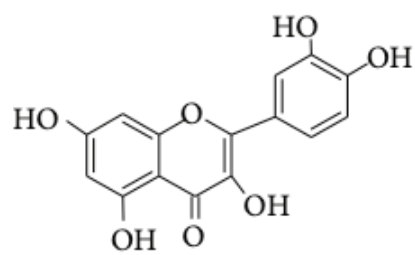

4. Flavonoid Glycoside (polyphenol, # of C: 20) (*assuming each -OH/=O is redox active*) EEC: 9 mol_{e^-} / (20 × 12 g_c) = 0.0375 $mmol_{e^-}/g_c$ = 37.5 mmol e^- g_c^{-1}	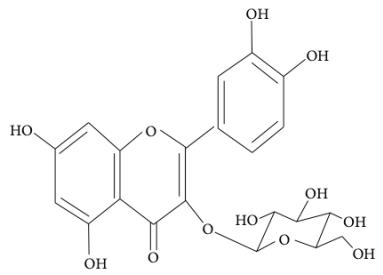

Results obtained show that under these conditions, enriched oxygenated functional groups on the polyphenol can give higher EECs than single ring compounds.

Theoretically, if there is a larger conjugated structure with more enriched redox moieties, it can be higher in EEC. Take this extreme case as example:

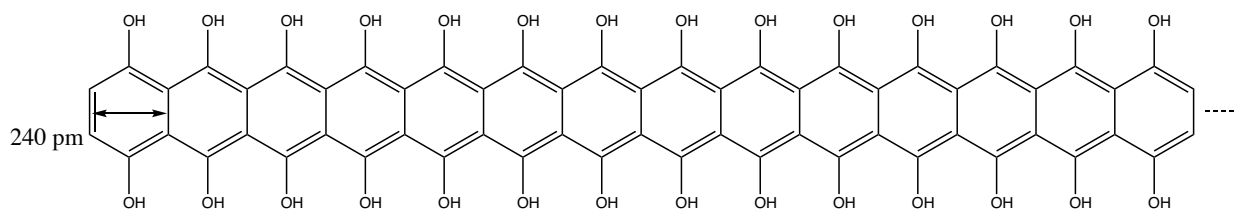

(*assuming each -OH/=O is redox active*)

Each benzene ring is 240 pm in length. Therefore, a 0.45 μm filter can allowa molecule that has ~1875 rings (0.45 × 10^6 pm / 240 pm = 1875). If the rings aligned as above, the total # of carbon in one mole would be 4 × 1875 + 2 = 7502. And if all rings were enriched with hydroxyl groups, the number of e^- transferred per mole would be 2 × 1875 e^- = 3750 e^-. The calculated EDC for this material would = 3750 mol_{e^-} / (7502 × 12) g_c = 42 mmol e^- g_c^{-1}.

Under these conditions, the larger the molecular weight, the higher the EEC value. The above molecule is just a hypothetical flat plain structure, while nanoparticles of 3D structure could be much larger than this, increasing the EDC/EAC to a certain extent. Still, the larger EEC of pyDOM obtained in Cao et al (2023)[1] at a level of hundreds to a thousand mmol e^- g_c^{-1} from SWV indicates that there might be other factors involved.

Table S1. Descriptor table of calibrant shuttles and used in this study.

Name (Common) [a]	Name (Abbrev.)	Sample ID Number [b]	Molecular Formula	Molar Mass (g mol^{-1})	SASA (A^2) [c]
p-Benzoquinone	BQ	106-51-4	C6H4O2	108.10	88.50
Juglone	Jug	481-39-0	C10H6O3	174.16	128.11
Napthoquinone Sulfonate	NQS	521-21-4	C10H5NaO5S	260.20	154.90
Ferrocene	Fc	102-54-5	C10H10Fe	186.04	61.05
1,4-Napthoquinone	NQ	130-15-4	C10H6O2	158.15	121.76
Anthraquinone	AQ	84-65-1	C14H10O2	208.22	155.02
1,2-Benzoquinone	BAQ	2498-66-0	C18H10O2	258.28	189.62
Anthroquinone Carboxylic Acid	AQCA	117-78-2	C15H8O4	252.23	181.54
Ascorbate	Asc	299-36-5	C6H7O6	176.12	114.83
Anthroquinone Disulfonate	AQDS	84-50-4	C14H6O8S2	366.30	227.24
Elliott Soil Humic Acid	ESHA	1S102H	N.A.	N.A.	N.A.
Leonardite Humic Acid	LHA	1S104H	N.A.	N.A.	N.A.
Pahokee Peat Fulvic Acid	PPFA	2S103F	N.A.	N.A.	N.A.
Pahokee Peat Humic Acid	PPHA	1S103H	N.A.	N.A.	N.A.
Suwanee River Fulvic Acid	SRFA	2S101F	N.A.	N.A.	N.A.
Suwanee River Natural Organic Matter	SRNOM	1R101N	N.A.	N.A.	N.A.

[a] All calibrant model compounds listed as their oxidized form.
[b] CAS-RN for calibrant model compounds; IHSS catalog numbers for NOMs.
[c] SASA = solvent accessible surface area (Connelly approximation).
N.A. = Not applicable.

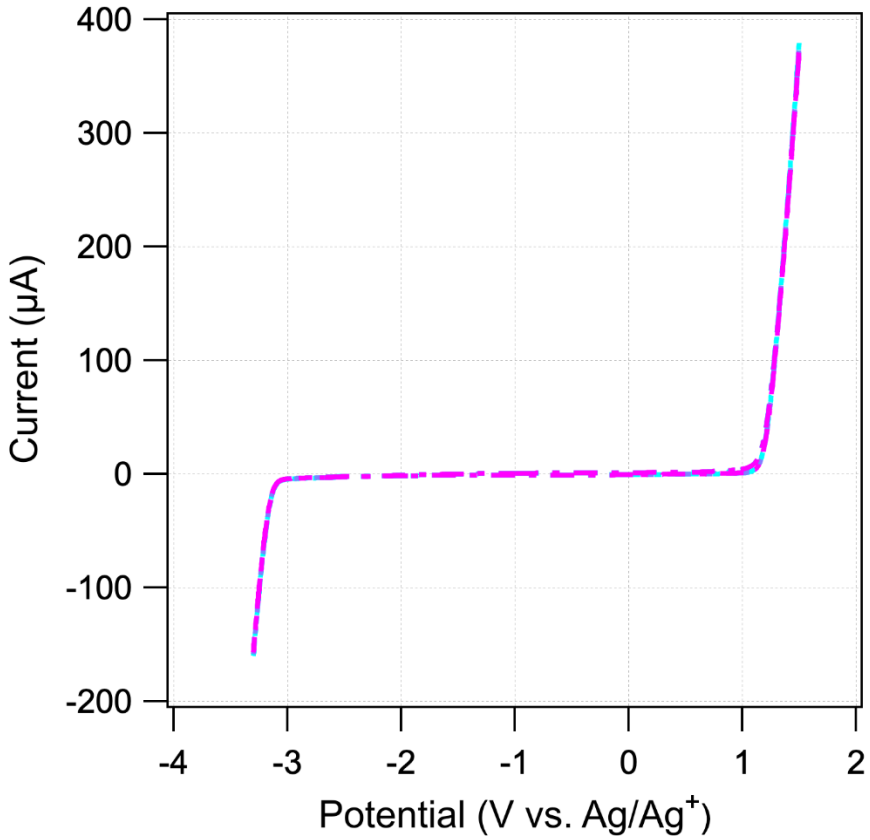

Figure S1. Stability window for 0.1M TBAPF in DMSO obtained via cyclic voltammetry. Data was obtained with both a glassy carbon working electrode and a platinum working electrode. Three scans were performed at 25 mV s^{-1} and the CVs overlap exactly.

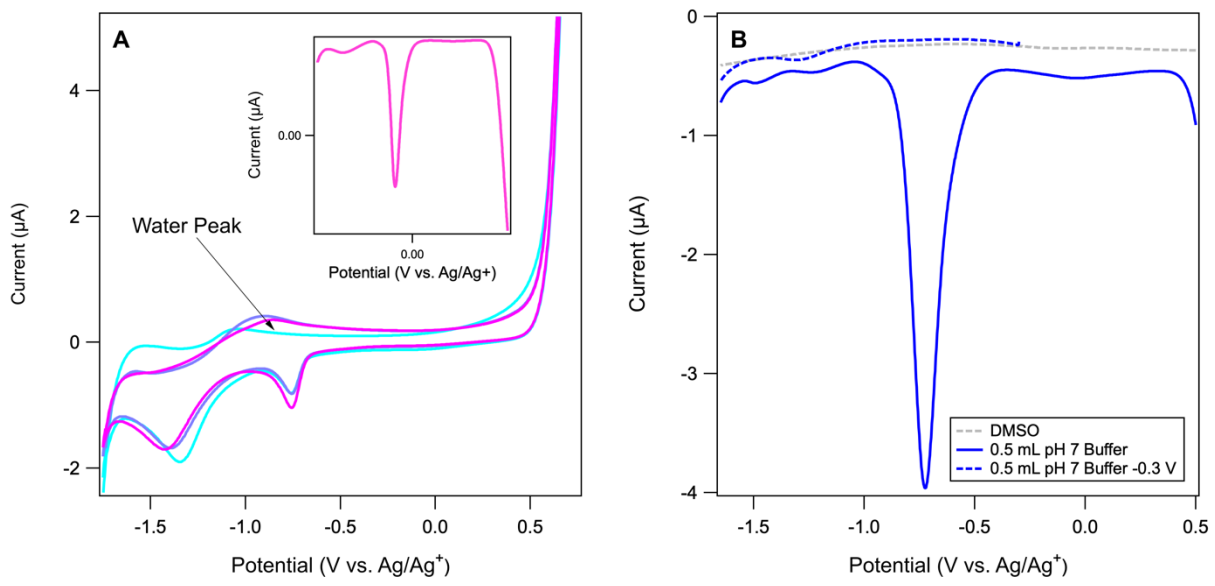

Figure S2. (**A**) Example of peak due to oxide reduction on a Pt working electrode during cyclic voltammetry, located at −0.7 V in the presence of a pyDOM sample, W300. The inset figure shows a cathodic SWV scan starting at +0.75 V. (**B**) Example of a peak due to oxide reduction on a Pt working electrode, located at −0.7 V. Note that the solid blue line corresponds to a cathodic scan of pH 7 phosphate buffer starting at +0.5 V, whereas the dotted blue line corresponds to a cathodic scan started at less positive overpotential (−0.3 V). For both, background scans were done on 5 mL of 0.1M TBAFP in DMSO alone (grey line), whereas data with peaks shown also had 0.5 mL of pH 7 phosphate buffer added as a cosolvent (total volume = 5.5 mL). The scan rate for both was 25 mV s^{-1} from 0.5 V to −1.75 V.

Table S2. Comparison of peak areas obtained for shuttles and NOM with a Pt and GC working electrode. Experiments performed with 0.1 M TBAFP in DMSO (5 mL DMSO and 0.5 mL spike of analyte dissolved in DMSO). Pt or GC working electrodes were used in a 3-electrode setup with a Ag/Ag^+ reference electrode, and Pt wire counter electrode. Scan rate was 25 mV/s, step size was 2 mV, and amplitude was 25 mV (SWV).

Sample	PA_{SWVa} [a]	PA_{SWVc} [a]	Conc.[b]	PA_{SWVa} [c]	PA_{SWVc} [c]	Conc.[d]
Fc	5.82E-07	6.03E-07	733 µM	8.73E-07	8.80E-07	588 µM
AQDS	4.60E-08	4.93E-08	506 µM	6.31E-07	7.78E-07	603 µM
SRNOM	5.82E-09	2.49E-08	300 $mg \cdot L^{-1}$	6.20E−07	9.17E−07	400 $mg \cdot L^{-1}$

[a] PA is total peak areas (full peaks included in scan window) (A·V) obtained with a Pt working electrode for both anodic and cathodic scans.
[b] Concentration of NOM in cell is $mg_{NOM} \cdot L^{-1}$.
[c] PA is total peak areas (full peaks included in scan window) (A·V) obtained with a GC working electrode for both anodic and cathodic scans.
[d] Concentration of NOM in cell is $mg_{NOM} \cdot L^{-1}$

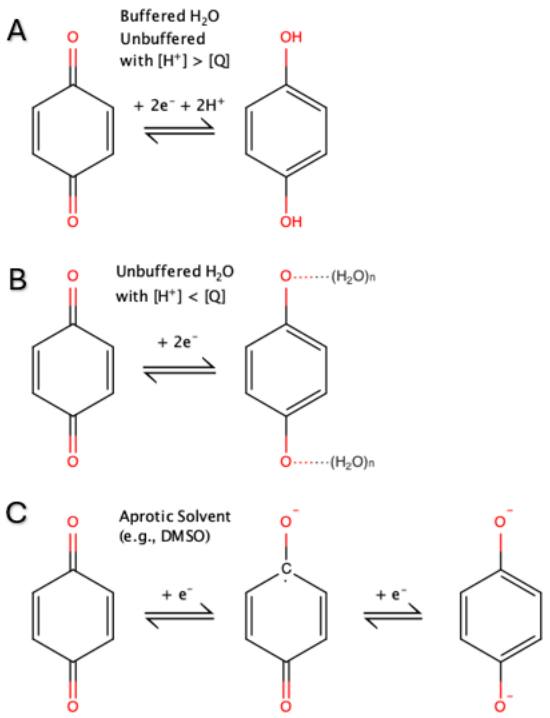

Scheme S1. Effect of solvent on quinone reduction, adapted from Quan et al.[2] (**A**) Coupled electron and proton transfer in buffered aqueous conditions or conditions where H^+ is in higher concentration than quinones. (**B**) Quinone reduction in unbuffered aqueous conditions. (**C**) Electron transfer (only) involving quinone reduction in an aprotic solvent.

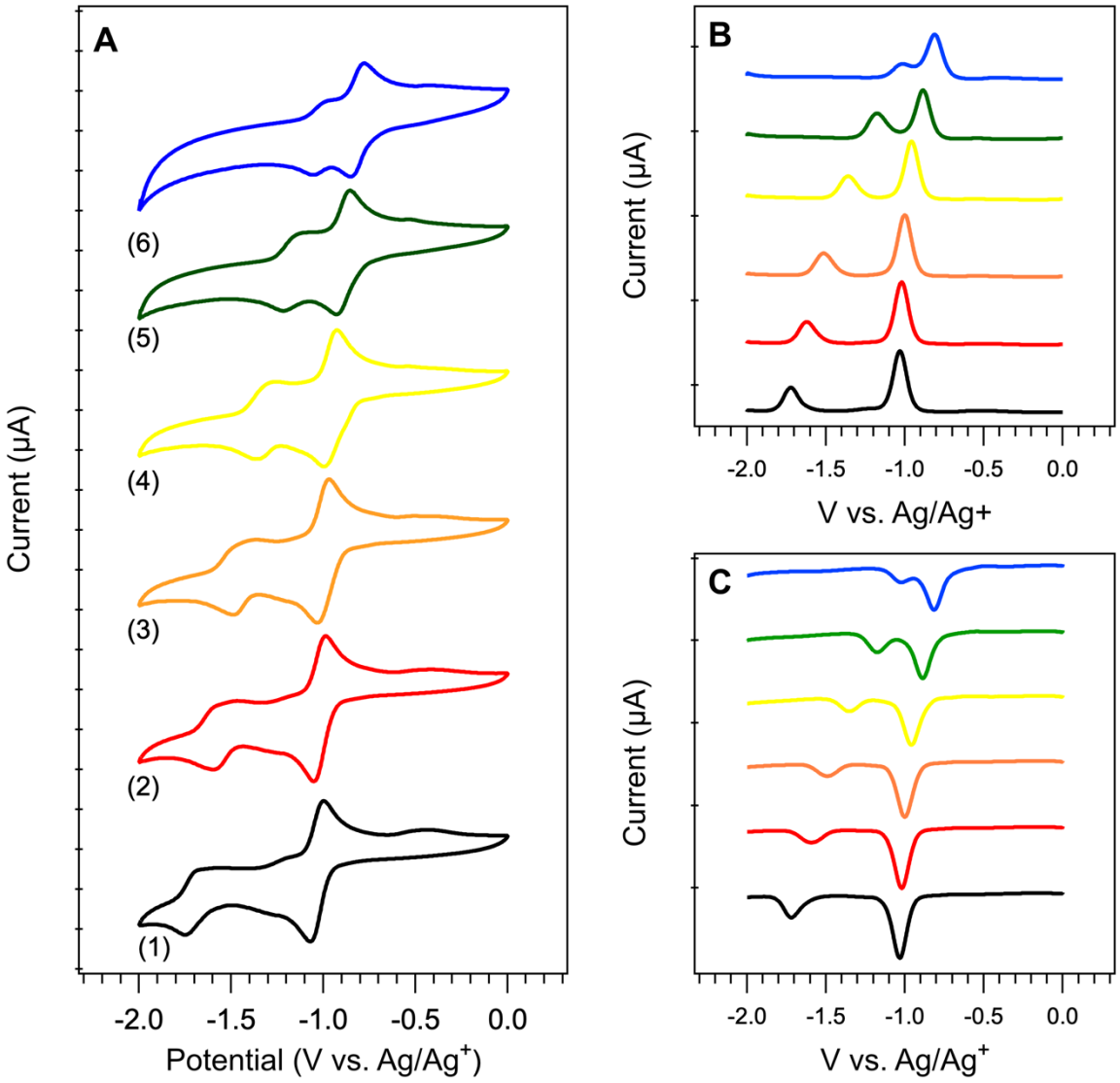

Figure S3. Influence of water cosolvent on redox properties of AQDS. (**A**) CVs of AQDS where (*1*) is 100% DMSO, (*2*) is 2 % H_2O (v/v), (*3*) is 5% H_2O, (*4*) is 10% H_2O, (*5*) is 17% H_2O, and (*6*) is 34% H2O. (**B**) Anodic SWV and (**C**) Cathodic SWV scans of AQDS. All of these experiments performed with a glassy carbon working electrode and 25 mV s^{-1} scan rate.

Text S2. Experimental determination of calibrant and NOM electro adsorption.

To determine the concentration of analytes sorbed to electrode surfaces, measured current data from cyclic voltammetry experiments were gathered following multiple cycles back and forth from applied potentials (−1.75 to +0.25 V versus Ag/Ag^+ for NOM samples, −2 to 0 V for many calibrants). CVs were performed between initial SWVs and final SWVs shown in **Figure 3.** Experiments, performed at sweep rates of 25 mV s^{-1}, were used to study charge that was measured after background correction (i.e., DMSO only) to determine either the surface coverage for adsorbed analyte or the number of moles converted in the diffusion-controlled electrolysis.[3, 4] The total electrolysis charge is given by the following:

$$Q_{total} = Q_{faradaic} + Q_{dl} + Q_{ads} = \frac{2nFAD^{\frac{1}{2}}Ct^{\frac{1}{2}}}{\pi^{\frac{1}{2}}} + Q_{dl} + nFA\Gamma \quad \text{(S1)}$$

where A is the electrode area (cm^2), D is the diffusion coefficient (cm^2 s^{-1}), C is the concentration (mol cm^{-3}), and Γ is the surface coverage of adsorbate (pmol cm^{-2}).

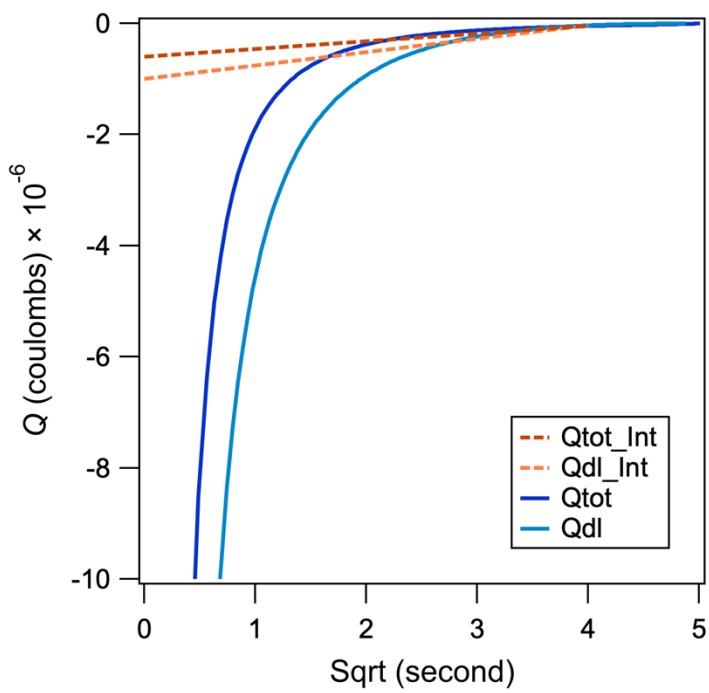

Figure S4. Coulometric plot showing sorption of NQS (dark blue, solid line, Qtot) to electrode (Qdl, light blue line) during anodic sweep. Qtot and Qdl were obtained by dividing current (A) by time (s) and plotting Q vs the square root of time (s).

Experimental data for Q was obtained by taking the difference between the intercept of total charge (Q_{tot}) and double layer charge (i.e., the blank measurement in DMSO without the model calibrant or NOM samples), Q_{dl}. Intercepts were determined by linearizing the current data towards the intercept. Data were obtained with both working electrodes both in negative and positive potential regions of scans in order to understand the difference of surface charges on sample monolayer adsorption (**Table S3**).

Table S3. Monolayer sorption parameters for calibrant (NQS) and NOM sample shown in Figure 2. Additionally, values for a pyDOM sample, W300, are shown.

Sample	WE [a]	E_{app} (V)	$\Gamma_{predictedsat}$ [b]	$\Gamma 1$ [c]	Conc. [d]
NQS	GC	−2	237	104	320 μM
NQS	GC	0	237	22	320 μM
NQS	Pt	−2	237	78	320 μM
NQS	Pt	0	237	31	320 μM
LHA	GC	−1.75	---	77	99 $mgC \cdot L^{-1}$
LHA	Pt	−1.75	---	85	99 $mgC \cdot L^{-1}$
W300	Pt	−1.75	---	146	105 $mgC \cdot L^{-1}$

[a] WE = working electrode.
[b] Units on all Γ are pmol cm^{-2}. Values are impossible to predict for NOM samples due to unknown theoretical molar concentrations.
[c] Measured monolayer concentration of sorbed molecules on electrodes. Units are in pmol cm^{-2} or mg of C cm^{-2} for NOMs. $\Gamma 1$ represents the first CV scan.
[d] Concentration of analyte in bulk. Units are μM, or $mgC \cdot L^{-1}$.

Text S3. Quantification and previous calibration details of SWV method.

In our previous study,[1] SWV results were quantified using two methodologies. Both methods initially involve integration of peak area (PA) from anodic and/or cathodic SWV scans as defined by equation eq S2:

$$\mathrm{PA}\ (\mathrm{A} \cdot \mathrm{V}) = \int_{E1}^{E2} \mathrm{I} \bullet \mathrm{dE} \tag{S2}$$

Where I is current (A), and E_1 and E_2 are the start and end potentials (V) for the peak, respectively. The SWV output results of PA are in the units of $A \cdot V$. Anodic peaks were used to obtain PA_{SWVa} and cathodic peaks were used to obtain PA_{SWVc}.

The resulting values of PA were divided by the scan rate (v; $V \cdot s^{-1}$) with eq S3 to obtain charge transferred (Q) in Coulombs (C), which could then be divided by the Faraday constant (F = 96,485 $C \cdot mol_{e-}^{-1}$) to give Q in moles of electrons with eq S4.

$$\mathrm{Q}\ (\text{in C}) = \mathrm{PA}/\mathrm{v} \tag{S3}$$

$$\mathrm{Q}\ (\text{moles of } \mathrm{e}^{-}) = \mathrm{Q}\ (\text{in C})/\mathrm{F} \tag{S4}$$

From here, Q can be normalized to the mass of organic carbon (NPOC; g_C) present in the sample, providing a method of EEC calculation we referred to as the "Faraday" method. Because disk electrodes commonly used in voltammetry do not react completely with the bulk analyte (in comparison to high-surface area electrodes designed for electrolysis), cell inefficiencies exist and are determined by operational factors (e.g., electrode surface area, diffusion-limited processes) that usually are best corrected using an experimentally determined response factor or calibration curve obtained with model compounds that have relatively ideal electrode responses.

In our earlier work,[1] calibration curves were obtained by SWV with varying concentrations of AQDS, chosen because it is a well-characterized electron-transfer mediator that displays suitable electrochemically reversible behavior in DMSO and is an analog for redox-active moieties in NOM.

For the dependent variable (y) in the calibration curve (**Figure S5A**), the directly measured electrode response (i.e., PA) was used. Originally, AQDS in SWV exhibited multiple

peaks during both the anodic and cathodic scans (**Figure S5A** and **5C**), yet only the largest, main peak was included for calculation of PA in our regression analysis. In our current investigation, we used all visible peaks. For the independent variable (x), the concentration of the mediator was expressed as X ($mol_{e-} \cdot L^{-1}$) and calculated using the experimentally prepared molar concentration of the mediator multiplied by the theoretical stoichiometry of the AQDS redox couple (i.e., n = 2).

The resulting regression equation and measured PAs for the experimental samples were used to back-calculate the X values. Subsequently, the electron donating or accepting capacities for SWV (EDC_{SWV} or EAC_{SWV}, respectively) for each experimental sample was obtained using the following equation:

$$\mathrm{EDC_{SWV}\ or\ EAC_{SWV}}\left(\mathrm{mol_{e^-}} \cdot \mathrm{g_C^{-1}}\right) = \mathrm{X}\,(\mathrm{mol_{e^-}} \cdot \mathrm{L^{-1}})/\mathrm{NPOC}\,(\mathrm{g_C} \cdot \mathrm{L^{-1}}) \quad \text{(S5)}$$

where the NPOC is determined from the sample analyzed in the electrochemical cell.

Table S4. *EDC* and *EAC* values obtained using MCA method, previous SWV calibration method, and values obtained in this study. All units are in $mmol_{e^-} \cdot g_C^{-1}$.

Sample	EDC_{MCA}[a]	EAC_{MCA}[a]	EDC_{SWV}[b]	EAC_{SWV}[b]	EDC_{SWV}[c]	EAC_{SWV}[c]	EEC_{SWV}[c]
$pyDOM_{W300}$	0.34	1.68	102	111	12.30	11.06	23.36
$pyDOM_{W400}$	0.54	2.61	110	186	13.33	11.99	25.32
$pyDOM_{W500}$	0.7	5.52	344	104	40.40	36.32	76.72
$pyDOM_{W600}$	0.17	4.21	159	121	19.27	17.32	36.59
$pyDOM_{W700}$	0.29	1.46	2600	517	261.94	235.53	497.46
$pyDOM_{G300}$	0.46	1.58	79.9	117	9.73	8.75	18.48
$pyDOM_{G400}$	0.73	2.75	334	212	39.21	35.26	74.47
$pyDOM_{G500}$	0.33	4.7	301	158	35.32	31.76	67.09
$pyDOM_{G600}$	0.31	4.93	296	170	35.00	31.47	66.48
$pyDOM_{G700}$	0.18	1.63	316	366	36.86	33.15	70.01
ESHA	1.04	2.11	51	30.2	8.39[d]	5.86[d]	14.25[d]
LHA	2.41	3.51	44.7	126	7.43[d]	22.88[d]	30.31[d]
PPFA	2.06	1.32	5.56	5.79	2.11[e]	3.18[e]	5.28[e]
PPHA	1.69	2.06	11.6	23.2	4.49[e]	12.88[e]	17.37[e]
SRFA	4.84	0.72	5.04	3.84	1.92[e]	2.13[e]	4.04[e]
SRNOM	2.56	1.08	7.57	6.42	2.87[e]	3.53[e]	6.40[e]

[a] MCA values obtained from Cao et al. [1]
[b] Values obtained from SWV using AQDS calibration method in Cao et al. [1]
[c] New values obtained from SWV using new calibration method. Ferrocene (Fc) η values obtained with a GC working electrode were used to correct for response factors of pyDOM samples.
[d] Napthoquinone-sulfonate (NQS) η values obtained with a GC working electrode were used to correct for response factors of these DOM samples.
[e] Anthraquinone Disulfonate (AQDS) η values obtained with a GC working electrode to correct for response factors of these DOM samples.

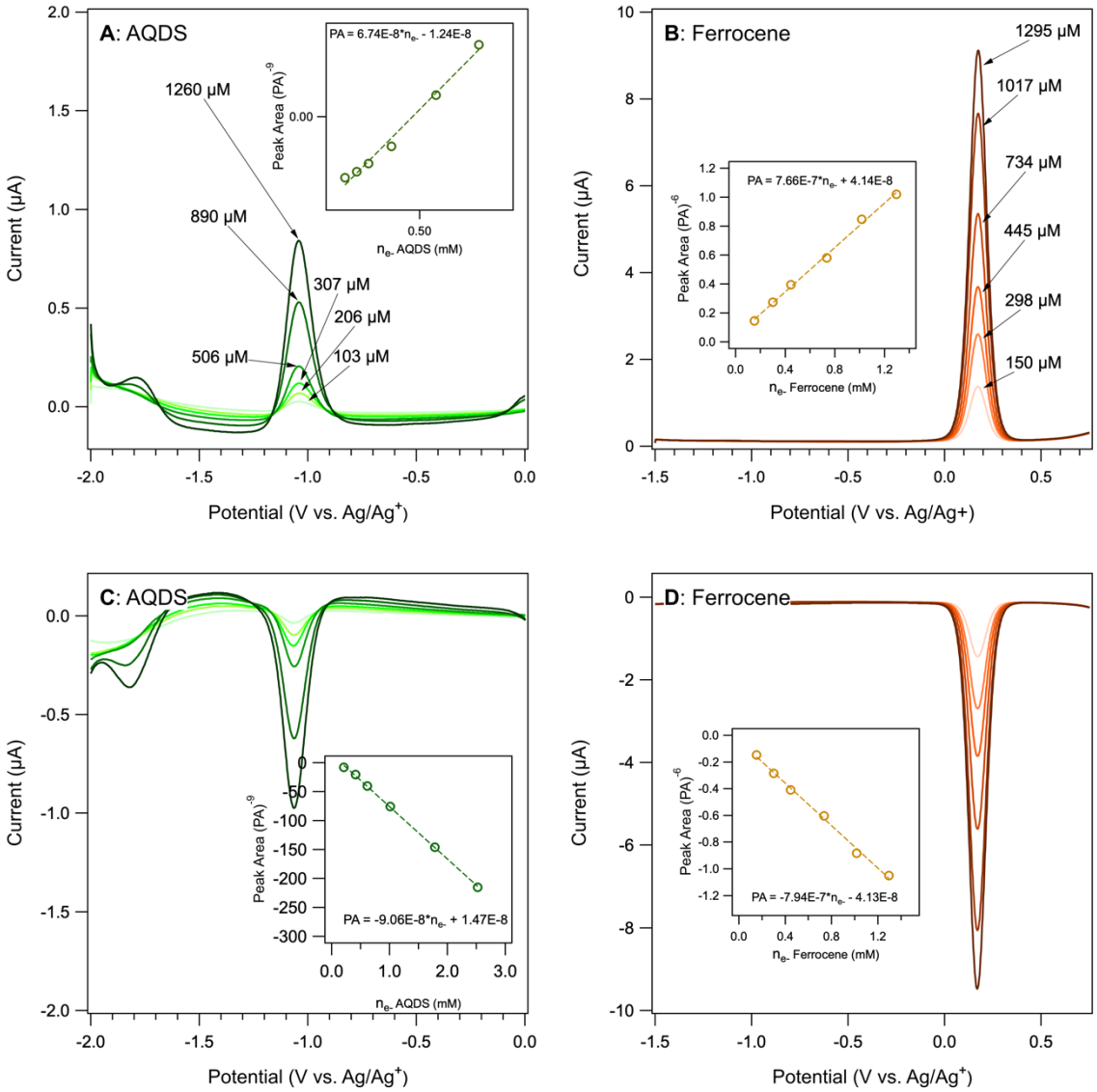

Figure S5. AQDS and ferrocene calibrations, with insets showing the resulting calibration curve (as PA versus n e^-). (**A**) Anodic AQDS SWV scans over increasing AQDS concentrations. (**B**) Cathodic SWV scans of AQDS. (**C**) Anodic SWV scans of ferrocene over increasing concentrations. (**D**) Cathodic SWV scans of ferrocene. All experiments were performed with a Pt working electrode in 0.1 M TBAFP/DMSO, and rate was 25 mV s^{-1}.

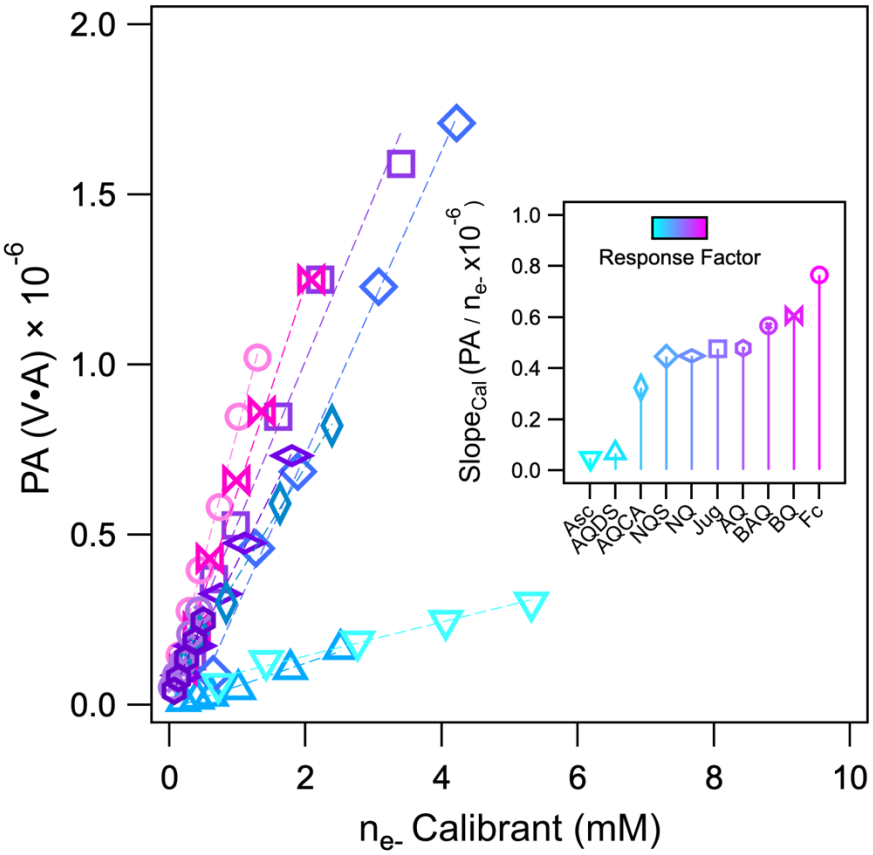

Figure S6. Calibration curves of various model quinones and other redox standards showing anodic peak area (PA) versus electron equivalents donated per mol of calibrant, assuming complete oxidation of each calibrant. The inset shows slopes (response factors) of the calibrants ranked from low to high. Note that this was the original method used in Cao et al.[1] to calibrate the working electrode for EEC quantitation.

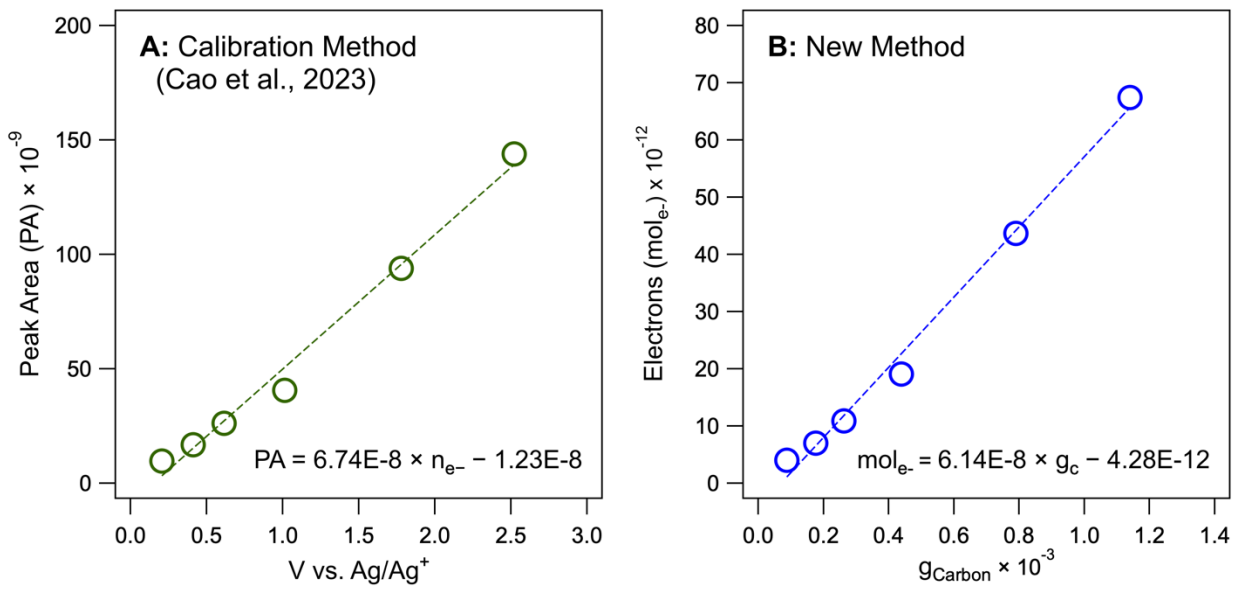

Figure S7. (**A**) Original method used in Cao et al.[1] to obtain EEC values. (**B**) New calibration method used to obtain EEC values in this study. Note that AQDS is the calibrant used in both examples, and that this specific comparison is of anodic SWV scans only (i.e., EDC). These two calibrations were performed with a Pt working electrode in 0.1 M TBAFP/DMSO, and rate was 25 mV s^{-1}.

Text S4. Revised calibration protocol details of SWV method.

The calibration curves used in our previous work were obtained with the quinone model redox shuttle AQDS, which exhibited a (relatively shallow in retrospect) slope of peak area (PA) versus electron equivalents. Using this calibration alone to calculate EECs for pyDOM and NOM (details in the SI of Cao et al.[1]) resulted in the relatively large values we reported in that study. Many aspects of that calculation were validated, but we did not investigate the effect of the calibrant choice on the results. In this study, we compare the effect of calibrations performed with AQDS versus a range of 9 other calibrants to better understand the influence of calibrant response factors on the quantitation of EECs.

New calibration curves were obtained for the 10 calibrants by performing SWV at varying shuttle concentrations and plotting electrons donated (*EDC*) or accepted (*EAC*) from the calibrants (mol e^-) versus their quantity in grams of carbon (g_C). The resulting plots were linear and plotted electrons detected from the integration of anodic (*EDC*) or cathodic (*EAC*) peak current on the y-axis, versus the calibrant mass (grams of carbon) in the cell on the x-axis, as shown in **Figure 4D** and discussed in the main text. The slopes of a resulting linear regression are as shown in **eq. S6** and **S7**:

$$EDC_{SWVCalibrant} = \frac{\int_{E1}^{E2} I \mathrm{d}E}{v \cdot F \cdot g_C} \tag{S6}$$

$$EAC_{SWVCalibrant} = \frac{\int_{E1}^{E2} I \mathrm{d}E}{v \cdot F \cdot g_C} \tag{S7}$$

where I is current (A), v is scan rate (V s^{-1}), F is the Faraday constant, and g_c is grams of carbon in the calibrants. As expected, calibrant slopes (mol e^- g_c^{-1}) obtained with shuttles ranged over several orders of magnitude (**Figure 4D**), indicating that the choice of calibrant has a significant influence on EEC quantitation.

In a conventional electrochemical cell used for potentiodynamic methods like SCV and SWV, as used in this study, the electrode response comes only from analyte within the boundary layer at the electrode tip. The it is expected that direct quantitation of electrons donated or accepted from calibrant peaks, as shown in **Figure 4A**, will result in EEC values that are

underestimated by orders of magnitude. In order to better understand this phenomenon, theoretical maximum EEC values (EEC_{Max}) were tabulated for all calibrants based on the maximum stoichiometric value of moles of electrons expected to be donated or accepted per gram of carbon in the calibrant (**eq S8**):

$$EEC_{Max} = \frac{mol\ e-}{n_{carbon} \cdot 12} \tag{S8}$$

where n_{carbon} represent the mols of carbon in each calibrant molecule and 12 is the molar mass of carbon. Cell efficiencies (η) were then tabulated as ratios of measured *EDC* and *EAC* values (**Table S5**) over their EEC_{Max} values (**eq S9**):

$$\eta_{Calibrant} = \frac{EDC_{SWV}}{EEC_{Max}} \tag{S9}$$

Calibrant η values for various shuttles we obtained with a Pt and GC working electrode were then plotted to understand conversion efficiencies of individual calibrants in our electrochemical cell in this study (**Figure 5**). Additionally, other values were tabulated from the literature to compare conversion efficiencies. On the whole, **Figure S9** shows very small η values obtained for calibrants with Pt and GC working electrode in our electrochemical cell setup, indicating that our electrode transfers electrons to only a very small proportion of the entire shuttle in the bulk. Within our method, trends show that ascorbate and AQDS are outliers with very low η values, possibly indicating an influence of lower compound diffusion coefficients (D_0) or heterogeneous electron transfer rate constants (k^0).

Likewise, **Figure S9** shows comparisons of η values obtained with different electrochemical cell configurations. In comparison to values obtained in this work, values obtained from other methods are higher. For instance, a cyclic voltammetry experiment with a graphite working electrode obtained a slightly higher η value, although the overall efficiency of the system is still low. Interestingly, values obtained with MCA (blue and purple markers in **Figure S9**), appear to give higher overall efficiencies. This is likely to be partially due to these electrotrolysis methods being potentiostatic, where current integration over long time periods (approximately 60 minutes) precludes kinetic influences with shuttles. Conversely, SWV and CV are potentiodynamic, where current response factors are not only influenced by the small size of the disk electrodes, but also kinetically influenced by D_0 and k^0 of shuttles.

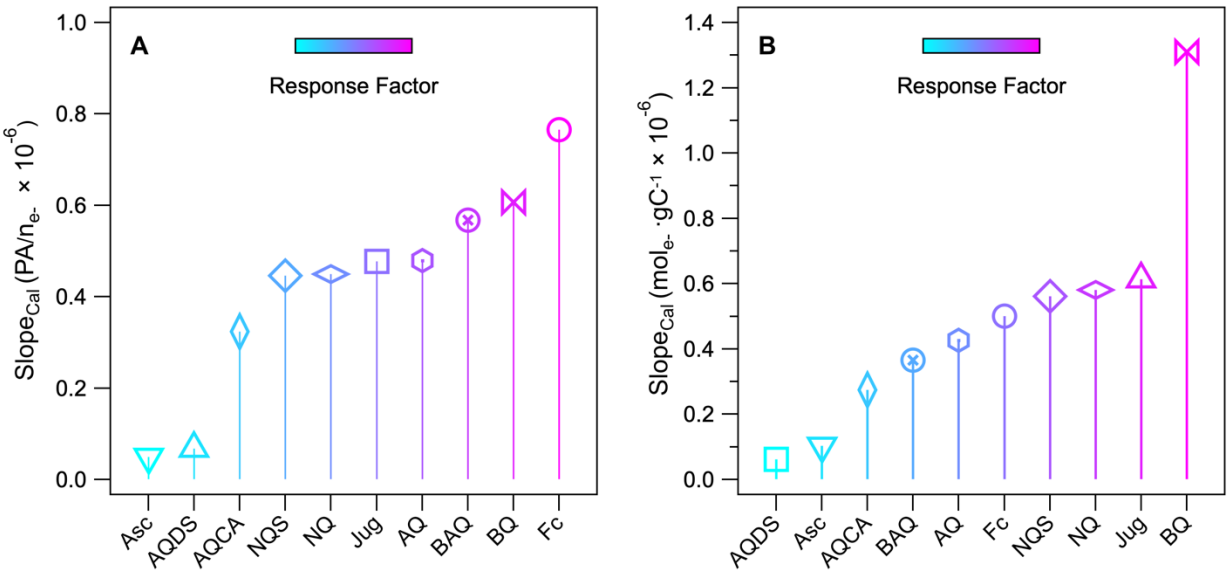

Figure S8. (**A**) Rank of calibration slopes obtained via the original method used in Cao et al.[1].(**B**) Rank of calibration slopes obtained in the current method. All calibration slopes shown were performed with a Pt working electrode in 0.1 M TBAFP/DMSO, and rate was 25 mV s^{-1}.

Table S5. Electrochemical parameters obtained for calibrant model compounds and some NOM samples used in this study.

Name (Electrode)[a]	Anodic Slope[b]	Cathodic Slope[b]	H^+/e^- [c]	*EDC*/ EAC_{Max}[d]	*EDC* η[e]	*EAC* η[e]	Half-Rxn 1[f]	D_0 1	k^0 1	Half-Rxn 2[g]	D_0 2	k^0 2
BQ	1.31E-06	-1.23E-06	2/2	2.80E-02	4.68E-05	4.39E-05	BQ_2^-/BQ^-	3.19E-06	---	BQ^-/BQ	4.06E-06	---
Jug	6.14E-07	-5.87E-07	2/2	1.67E-02	3.68E-05	3.51E-05	Jug_2^-/Jug^-	6.24E-05	---	Jug^-/Jug	1.27E-07	---
NQS	5.60E-07	-5.38E-07	2/2	1.67E-02	3.36E-05	3.22E-05	NQS_2^-/NQS^-	7.82E-07	---	NQS^-/NQS	2.14E-06	---
$NQS_{(GC)}$	1.82E-06	-1.37E-06	2/2	1.67E-02	1.09E-04	8.20E-05	NQS_2^-/NQS^-	1.06E-06	---	NQS^-/NQS	2.62E-06	---
Fc	5.01E-07	-5.18E-07	0/1	8.33E-03	6.01E-05	6.22E-05	Fc/Fc^+	7.64E-07	6.20E-11	---	---	---
$Fc_{(GC)}$	1.07E-06	-1.19E-06	0/1	8.33E-03	1.28E-04	1.43E-04	Fc/Fc^+	8.13E-07	8.17E-09	---	---	---
NQ	5.81E-07	-6.49E-07	2/2	1.67E-02	3.48E-05	3.89E-05	NQ_2^-/NQ^-	1.24E-06	---	NQ^-/NQ	9.24E-08	---
AQ	4.27E-07	-4.33E-07	2/2	1.19E-02	3.59E-05	3.64E-05	AQ_2^-/AQ^-	4.46E-07	---	AQ^-/AQ	8.55E-09	---
BAQ	3.66E-07	-3.96E-07	2/2	9.26E-03	3.95E-05	4.28E-05	BAQ_2^-/BAQ-	4.94E-07	---	BAQ^-/BAQ	3.80E-08	---
AQCA	2.75E-07	-2.91E-07	2/2	1.11E-02	2.48E-05	2.62E-05	$AQCA_2^-/AQCA^-$	8.74E-07	---	$AQCA^-/AQCA$	3.92E-07	---
Asc	1.03E-07	-8.73E-08	2/2	2.78E-02	3.71E-06	3.14E-06	Asc·/DHA	---	---	Asc/Asc·	7.90E-08	---
$Asc_{(GC)}$	---	---	2/2	2.78E-02	---	---	Asc·/DHA	4.39E-09	---	Asc/Asc·	2.84E-08	---
AQDS	6.14E-08	-8.24E-08	2/2	1.19E-02	5.16E-06	6.92E-06	$AQDS_2^-/AQDS^-$	2.94E-08	5.11E-05	$AQDS^-/AQDS$	6.82E-08	5.66E-04
$AQDS_{(GC)}$	4.80E-07	-5.78E-07	2/2	1.19E-02	4.03E-05	4.86E-05	$AQDS_2^-/AQDS^-$	4.92E-08	4.44E-06	$AQDS^-/AQDS$	3.24E-07	5.53E-07
SRNOM	4.45E-09	---	NA	NA	---	---	NA	1.47-09	3.76E-06	NA	2.39E-10	---
W300	---	---	NA	NA	---	---	NA	---	4.46E-05	NA	---	---

[a] Subscript beside abbreviated name refers to electrode used for measurement.
[b] Slopes are in units of mol e^-·g C^{-1}
[c] Stoichiometric proton/electron transfer of each calibrant model compound. Note that proton transfer is not applicable in DMSO.
[d] Theoretical maximum number of electrons donated (*EDC*) or accepted (*EAC*) per mol of calibrant model compound. Units are mol e^- gC^{-1}.
[e] Efficiency term for calibrant model compounds derived from EDC_{SWV}/EDC_{Max} or EAC_{SWV}/EAC_{Max}, respectively. Units are mol e^- gC^{-1}.
[f] Half-reaction 1 corresponds to first redox-couple of calibrant that proceeds during anodic scans that start at –2 V. D_0 1 and k_0 1 correspond to half-reaction 1.
[g] Half-reaction 2 corresponds to second redox-couple of calibrant that proceeds during anodic scans that start at –2 V. D_0 2 and k_0 2 correspond to half-reaction 2.

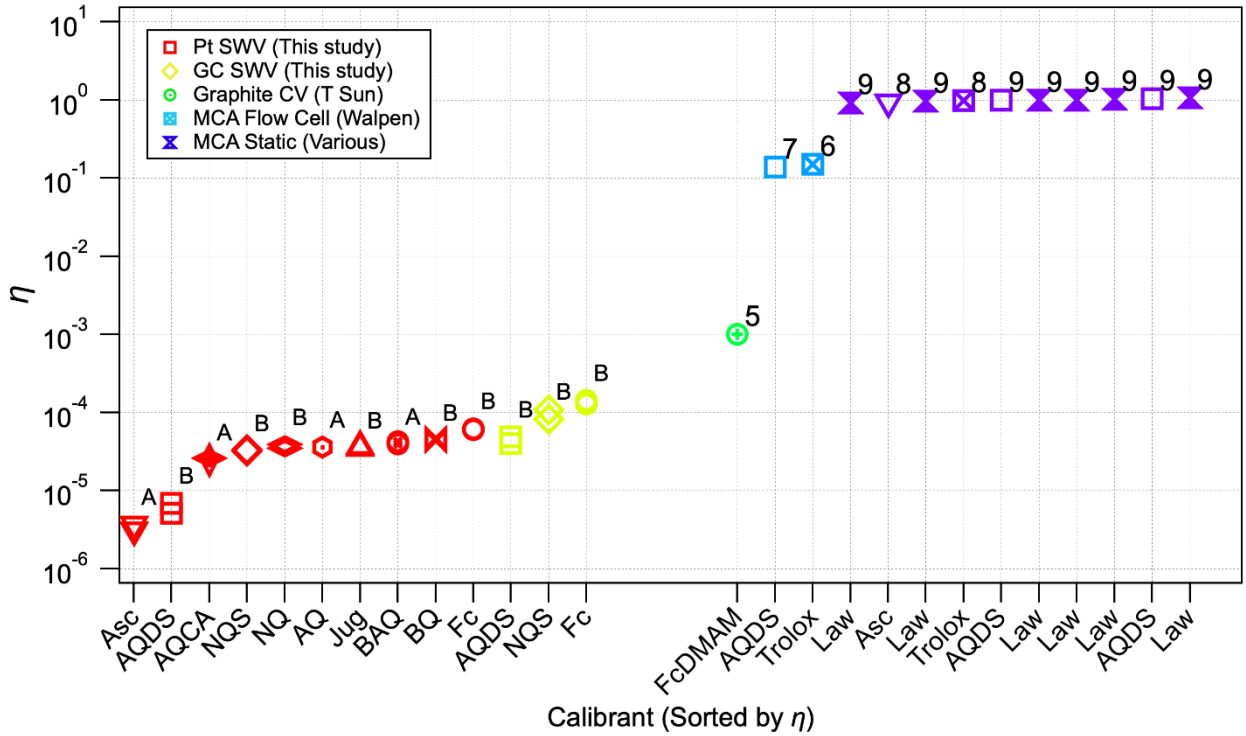

Figure S9. All compiled efficiency (η) data versus the calibrant model compound used in the measurement sorted by the corresponding values of η of individual calibrants sorted based on their η values. Marker shape and color represent the electrochemical cell configuration and method. Superscript letters represent the source of each value and correspond to *EDC* η (a) and *EAC* η (b) located in Table S5. The superscript numbers denote values obtained from other studies and correspond to references below.

Text S5. Linking hydrodynamic properties of calibrants to response factors within our cell.

Because it is well known surface area to volume (A/V) ratios ($cm^2\ mL^{-1}$) of electrochemical cells can influence working electrode current efficiency,[5] η values were plotted versus calculated ratios for working electrodes in this work, as well as examples from literature. **Figure S9** shows a relationship between these two properties, demonstrating that A/V is a dominant operational variable in controlling η values. Based on tabulated literature data, it appears that a tailing effect may occur as η values approach 1, as A/V ratios that continually increase after this cannot enhance theoretical maximum efficiencies for electron transfer, although this may account for electrolysis reactions where >100% of electron transfer to the analyte is achieved. Furthermore, **Figure S10** shows that choice of calibrant has a secondary, minor influence on cell efficiencies, based on the smaller distribution of η values obtained within individual method clusters.

From **Figure S10**, it is also possible to see that, while A/V ratios are the predominant variable influencing η values, the distribution of low values obtained via SWV and CV versus high η values obtained via chronoamperometric methods (difference of approximately 3 orders of magnitude) indicates that the choice of potentiodynamic versus potentiostatic methods is the second most important factor controlling cell efficiency when calculating overall η for NOM EECs. Finally, within potentiodynamic methods used in this study (upper left of **Figure S11**), a distribution of efficiencies ranging approximately two orders of magnitude indicates that choice of calibrant ranks third in order of influence on cell efficiency when tabulating EECs of calibrants and NOM. Interestingly, the wider distribution of η values obtained with our potentiodynamic experiments (red and yellow markers) accentuates the influence of electron transfer kinetics on electron exchange during SWV experiments, highlighting the sensitivity of the SWV method to capture kinetic effects of electron transfer in addition to quantitation of electron transfer.

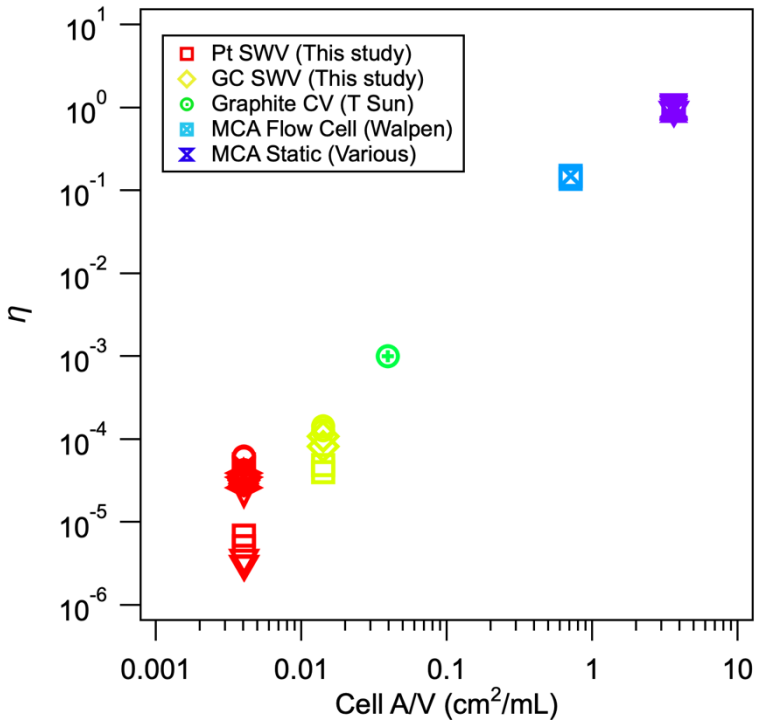

Figure S10. Efficiency (η) values plotted versus their working electrode surface area (cm^2) to volume (mL) ratios. Markers are related to individual calibrants and correspond to the same calibrants in Figure S9. Note that the volume for graphite CV [6] is inferred since this information was not directly obtainable in the text.

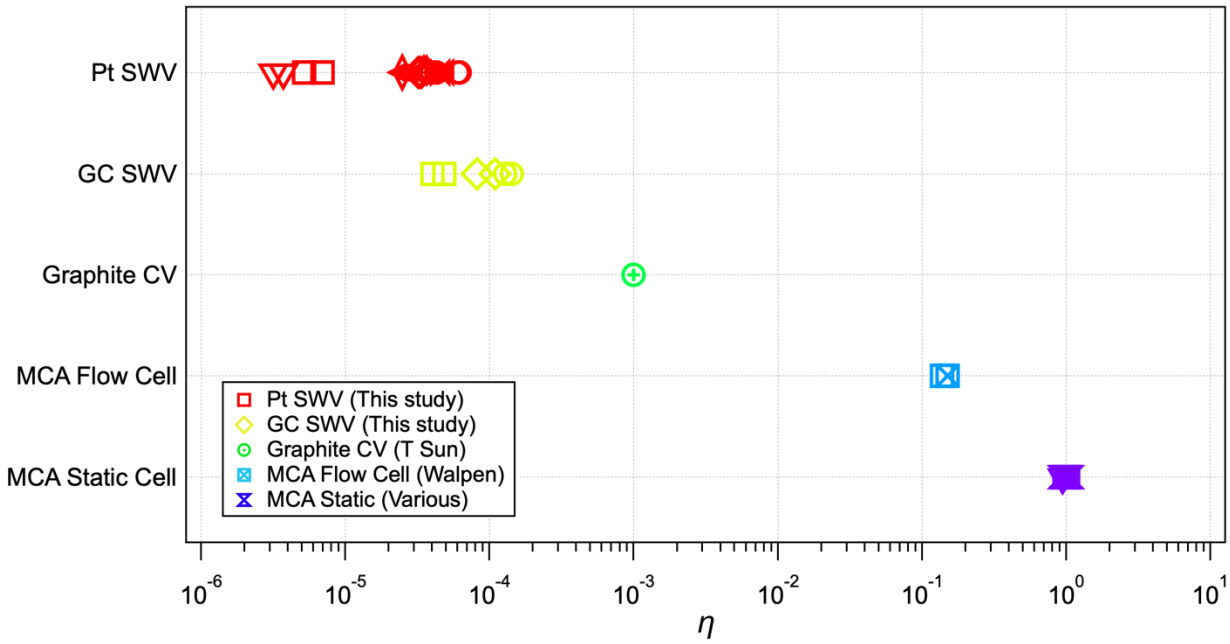

Figure S11. Efficiency (η) of individual calibrant model compounds in this study and literature sorted based on their electrochemical cell configurations. Individual calibrants have the same markers as Figure S9. Colors correspond to electrochemical cell configurations as in Figure S9.

Text S6. Determining diffusion coefficients and electron transfer kinetics of calibrants and NOM in our cell.

Initially, we hypothesized that minor differences in slopes were due to differences in shuttle diffusion coefficients, while larger differences in slopes were due to chemical interactions between shuttles and working electrodes surfaces or within the DMSO. To test this hypothesis, apparent diffusion coefficients (D_0) were obtained via anodic and cathodic peak current data from cyclic voltammograms during our SCV/SWV experimental protocol.[7] From CVs, apparent diffusion coefficients (D_0) were obtained via two approaches: (*i*) cyclic voltammograms from compiled calibrant model compound data over increasing concentrations (**Text S3, Table S5**), or (*ii*) scan rate tests (**Figure S12)**. Scan rate tests were used on two model calibrants (Ferrocene and AQDS), along with one NOM sample (SRNOM) to validate diffusion-controlled behavior seen with calibrants over increasing concentrations (approach *i*). Peak current showed a linear dependance on centration, when used in the **eq S10**

$$i_{\mathrm{p}} = 269000 \text{ x } n^{\frac{3}{2}} \text{ x } A \text{ x } D_0^{\frac{1}{2}} \text{ x } C \text{ x } v^{\frac{1}{2}} \tag{S10}$$

where i_{p} is the peak current, n (1 in this case) is the number of electrons transferred by individual redox couples (e.g., Q^{2-}/Q^{-} and Q^{-}/Q) within shuttles, A (0.071 cm^2 for the GC working electrode, 0.020 cm^2 for the Pt working electrode) is the electrode surface area, C is the initial shuttle concentration (mol/cm^3) in bulk, v indicates the scan rate (V/s), and D_0 is the apparent diffusion coefficient.

Unsurprisingly, Ferrocene and AQDS during scan rate experiments showed a linear dependence on the square root of the potential scan rate (AQDS data shown in **Figure S12B and S12E**), making it comply with the Randles-Sevcik equation (**eq S10**), and was also confirmed by **eq S11**

$$D_0 = \left(\frac{Slope}{269000 \text{ x } n^{\frac{3}{2}} \text{ x } A \text{ x } C}\right)^2 \tag{S11}$$

where we used slopes to determine D_0. For quinone calibrant model compounds, we derived two distinct D_0 values for each reversible redox couple (2 per quinone). D_0 values for calibrants obtained with Pt and GC working electrodes showed good agreement, indicating accurate measurements (**Table S5**).

To obtain heterogeneous electron transfer rate constants (k^0) of AQDS, Ferrocene (i.e., two calibrants with low and high response factors), and SRNOM, we measured the peak separation between reduction and oxidation peak current from CVs to use in **eq S11**:

$$k^0 = \frac{e^{Intercept}}{0.227 \text{ x } n \text{ x } F \text{ x } A \text{ x } C} \quad \text{(S12)}$$

where the intercept was obtained from linear fittings of the natural logarithm of the absolute values of the peak current (ln $|i_p|$) and overpotential (i.e., difference between calibrant peak potentials and their formal potentials across varying scan rates (**Figure S12**). Diffusion coefficients and k^0 obtained for calibrants are listed in **Table S5**.

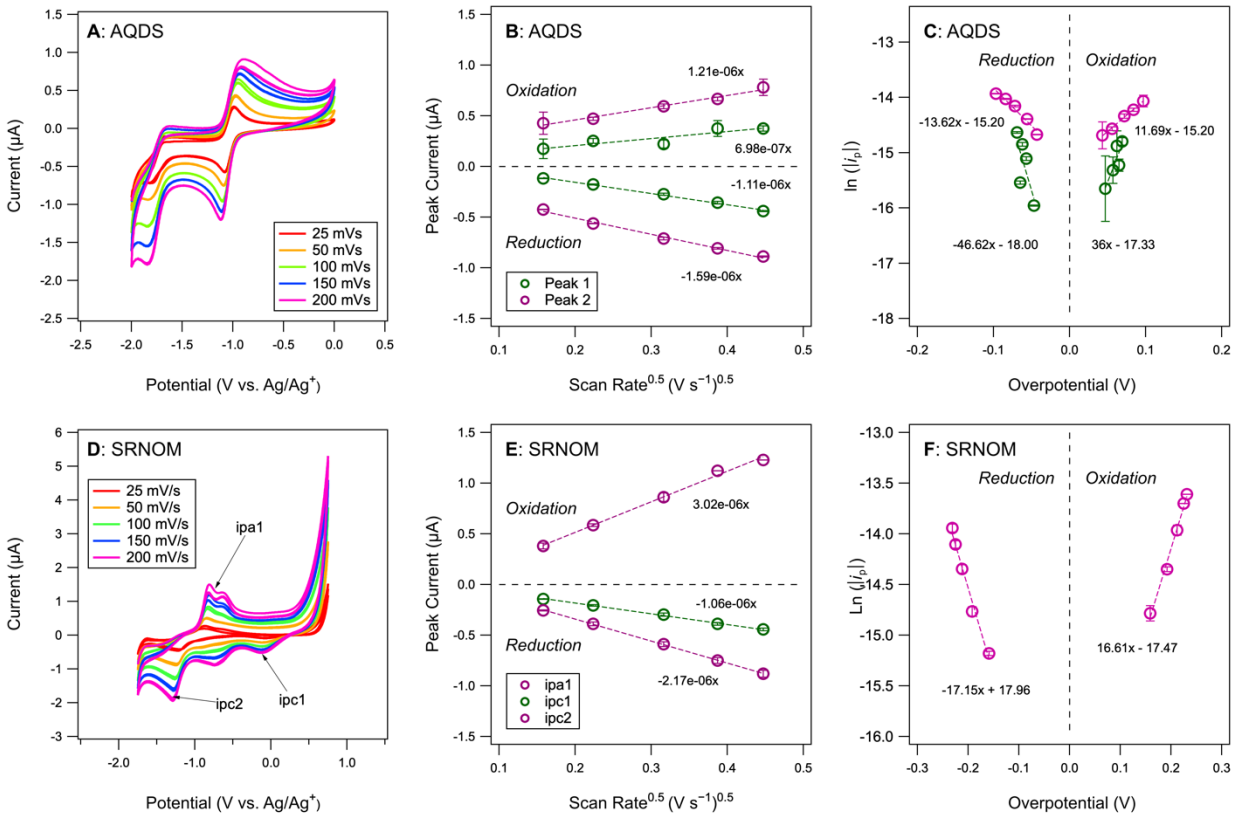

Figure S12. Analysis of calibrant model compound and NOM diffusion coefficients. (**A**). AQDS current response with varying scan rates. (**B**) Peak current response from (A) plotted versus the square root of scan rates. Slopes were used to obtain D_o values. Note that diffusion coefficient values were obtained for two reversible peaks, each pertaining to an AQDS redox couple. (**C**) Tafel plot of peak current responses from (A) plotted versus peak overpotentials. Slope intercepts were used to calculate k^0. (D) SRNOM current response with varying scan rates. (**E**) Peak current responses from (D) plotted versus the square root of scan rates. In comparison to AQDS, only one quasi-reversible peak is present (labeled as ipa1 and ipc2), along with another standalone cathodic peak (labeled as ipc1). All measurements shown here were performed with a Pt working electrode in 0.1M TBAFP/DMSO solutions. (**F**) Tafel plot of peak current responses from (D) plotted versus peak overpotentials. Slope intercepts were used to calculate k^0. All measurements shown here were performed with a Pt working electrode in 0.1M TBAFP/DMSO solutions.

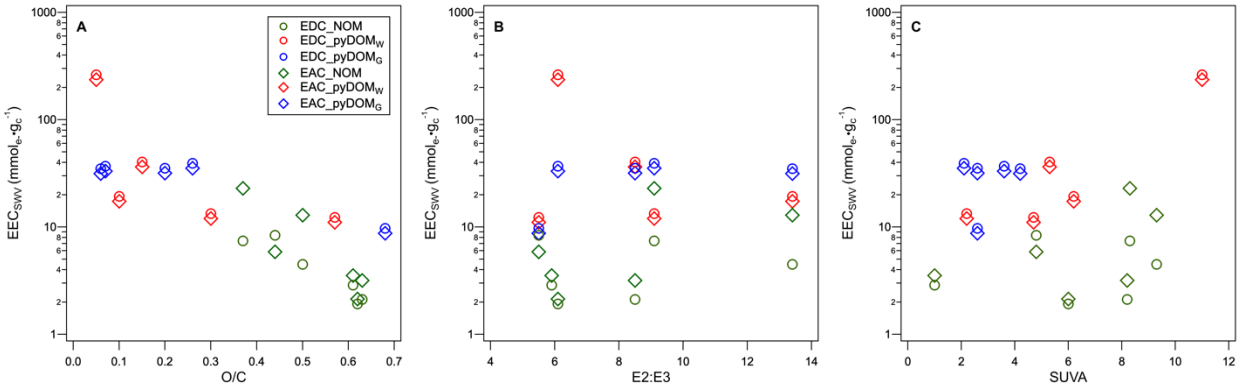

Figure S13. (**A**) NOM and pyDOM EEC values plotted versus O/C ratios. (**B**) NOM and pyDOM EECs plotted versus *E2:E3* values. (**C**) NOM and pyDOM EECs plotted versus SUVA values. Data are from Tables S4 and S6.

Table S6. NOM bulk molecular properties obtained from spectroscopy in Cao et al. [1]

Sample	O/C[a]	E2:E3[b]	SUVA[c]
$pyDOM_{W300}$	0.57	5.5	4.7
$pyDOM_{W400}$	0.3	9.1	2.2
$pyDOM_{W500}$	0.15	8.5	5.3
$pyDOM_{W600}$	0.1	13.4	6.2
$pyDOM_{W700}$	0.05	6.1	11
$pyDOM_{G300}$	0.68	5.9	2.6
$pyDOM_{G400}$	0.26	6.9	2.1
$pyDOM_{G500}$	0.2	9.2	2.6
$pyDOM_{G600}$	0.06	12.1	4.2
$pyDOM_{G700}$	0.07	6.7	3.6
ESHA	0.44	3.1	4.8
LHA	0.37	3.2	8.3
PPFA	0.63	4.2	8.2
PPHA	0.5	3.1	9.3
SRFA	0.62	4.3	6
SRNOM	0.61	5.1	1

[a] O/C values obtained from Cao et al. [1]
[b] E2:E3 values obtained from Cao et al. [1]
[c] SUVA values obtained from Cao et al. [1]

References

1. H. Cao, A. S. Pavitt, J. M. Hudson, P. G. Tratnyek and W. Xu. Electron exchange capacity of pyrogenic dissolved organic matter (pDOM): Complementarity of square-wave voltammetry in DMSO and mediated chronoamperometry in water. *Environ. Sci. Proc. Impacts*, 2023, **25**, 767-780 [DOI: 10.1039/d3em00009e].

2. M. Quan, D. Sanchez, M. F. Wasylkiw and D. K. Smith. Voltammetry of quinones in unbuffered aqueous solution: Reassessing the roles of proton transfer and hydrogen bonding in the aqueous electrochemistry of quinones. *J. Am. Chem. Soc.*, 2007, **129**, 12847-12856 [DOI: 10.1021/ja0743083].

3. J. Xu, Q. Chen and G. M. Swain. Anthraquinonedisulfonate electrochemistry: A comparison of glassy carbon, hydrogenated glassy carbon, highly oriented pyrolytic graphite, and diamond electrodes. *Anal. Chem.*, 1998, **70**, 3146-3154 [DOI: 10.1021/ac9800661].

4. M. P. Soriaga and A. T. Hubbard. Determination of the orientation of adsorbed molecules at solid-liquid interfaces by thin-layer electrochemistry: Aromatic compounds at platinum electrodes. *J. Am. Chem. Soc.*, 1982, **104**, 2735-2742 [DOI: 10.1021/ja00374a008].

5. N. Petrovic, B. K. Malviya, C. O. Kappe and D. Cantillo. Scaling-up electroorganic synthesis using a spinning electrode electrochemical reactor in batch and flow mode. *Org. Process Res. Dev.*, 2023, **27**, 2072-2081 [DOI: 10.1021/acs.oprd.3c00255].

6. T. Sun, B. D. A. Levin, J. J. L. Guzman, A. Enders, D. A. Muller, L. T. Angenent and J. Lehmann. Rapid electron transfer by the carbon matrix in natural pyrogenic carbon. *Nature Comm.*, 2017, **8**, 14873 [DOI: 10.1038/ncomms14873].

7. Y. Bai, T. Sun, L. T. Angenent, S. B. Haderlein and A. Kappler. Electron hopping enables rapid electron transfer between quinone-/hydroquinone-containing organic molecules in microbial iron(III) mineral reduction. *Environ. Sci. Technol.*, 2020, **54**, 10646-10653 [DOI: 10.1021/acs.est.0c02521].